Supplemental information

Article title.

Advanced LSI-based amperometric sensor array with light-shielding structure for effective removal of photocurrent and mode selectable function for individual operation of 400 electrodes

Author's names.

Kumi Y. Inoue,[*ab] Masahki Matsudaira,[b] Masanori Nakano,[a] Kosuke Ino,[a]
Chika Sakamoto,[a] Yusuke Kanno,[a] Reyushi Kubo,[a] Ryota Kunikata,[c] Atsushi Kira,[c]
Atsushi Suda,[c] Ryota Tsurumi,[d] Toshihito Shioya,[d] Shinya Yoshida,[f]
Masanori Muroyama,[be] Tomohiro Ishikawa,[be] Hitoshi Shiku,[abf] Shiro Satoh,[b]
Masayoshi Esashi,[bf] and Tomokazu Matsue[*abf]

Affiliations.

[a]Graduate School of Environmental Studies, Tohoku University, 6-6-11 Aramaki-Aza-Aoba, Aoba-ku, Sendai 980-8579, Japan

[b]Micro System Integration Center (μSIC), Tohoku University, 519-1176 Aramaki-Aza-Aoba, Aoba-ku, Sendai 980-0845, Japan

[c]Japan Aviation Electronics Industry, Limited, 1-21-2 Dogenzaka, Shibuya-ku, Tokyo 150-0043, Japan

[d]Toppan Technical Design Center Co., Ltd., 1-5-1, Taito, Taito-ku, Tokyo 110-0016, Japan

[e]Graduate School of Engineering, Tohoku University, 6-6-01 Aramaki-Aza-Aoba, Aoba-ku, Sendai 980-8579, Japan

[f]The World Premier International Research Center Advanced Institute for Materials Research (WPI-AIMR), Tohoku University, 2-1-1 Katahira, Aoba-ku, Sendai 980-8579, Japan

Voltammetric performance of 2G Bio-LSI

The fundamental voltammetric properties of 2G Bio-LSI were estimated using cyclic voltammetry. Figure S1 shows the cyclic voltammograms of 400 simultaneous measurements for 2.0 mM ferrocenemethanol ($FcCH_2OH$) in 0.1 M KCl at a scan rate of 20 mV/s. The 400 working electrodes were all Au, with a diameter of 40 μm. The shapes of the cyclic voltammograms with Bio-LSI were in good agreement with the simulation results in the previous paper.[10] Almost uniform cyclic voltammograms for 400 electrodes were obtained with a coefficient of variance of 4.1% for the currents of 400 cyclic voltammograms at 0.60 V. This result indicates that the 400 electrodes of 2G Bio-LSI work uniformly on the amperometric and voltammetric measurements with theoretical electrochemical behaviors. The sigmoidal shape of the voltammograms also

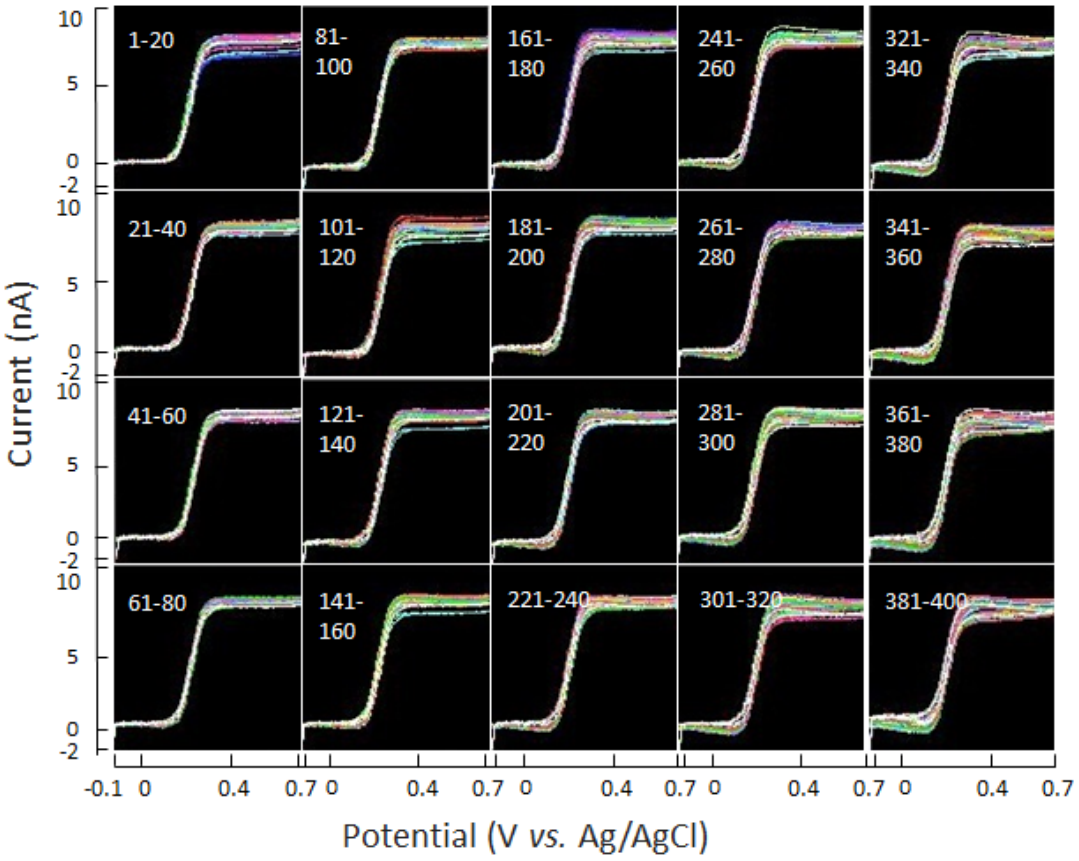

Figure S1. Typical cyclic voltammograms of simultaneous 400-point measurements using 2G Bio-LSI for 2 mM FcOH in 0.1 M KCl. The scan rate was 20 mV/s. The numbers shown in the graphs are the labels of the electrodes. Each of the 20 voltammograms of the same column is shown in one graph.

indicates that the electrodes on Bio-LSI have microelectrode-like properties of spherical diffusion in the mass transport process. Although microelectrodes require highly sensitive current detectors owing to the low current, they offer significant advantages in amperometric measurements such as high mass transport density, small double-layer capacitance, and small ohmic drop. The detection limit of our Bio-LSI is less than 1 pA, which is enough to conduct amperometric sensing with the microelectrodes.

Performance of in the electrometer mode

We examined the performance in the electrometer mode of 2G Bio-LSI using mixture solutions of potassium hexacyanoferrate(III) ($[Fe(CN)_6]^{3-}$; Wako Pure Chemical Industries, Japan) and potassium hexacyanoferrate(II)trihydrate ($[Fe(CN)_6]^{4-}$; Sigma-Aldrich, USA). $[Fe(CN)_6]^{3-}$ and $[Fe(CN)_6]^{4-}$ are the redox couple for which the molecular ratio at the surface of the electrode gives the rest potential as the following Nernst equation:

$$E = E^{0'} + 0.0592 \times \log_{10} \frac{C([Fe(CN)_6]^{3-})}{C([Fe(CN)_6]^{4-})} \quad (at\ 25°C) \qquad \cdots\cdots (S1)$$

where E is the rest potential of the electrode (V), $E^{0'}$ is the formal redox potential of the $[Fe(CN)_6]^{3-}$/ $[Fe(CN)_6]^{4-}$ redox couple (V), $C([Fe(CN)_6]^{3-})$ is the concentration of $[Fe(CN)_6]^{3-}$ (M), and $C([Fe(CN)_6]^{4-})$ is the concentration of $[Fe(CN)_6]^{4-}$ (M). We prepared 20 mM $[Fe(CN)_6]^{3-}$ in 0.1 M KCl solution and 20 mM $[Fe(CN)_6]^{4-}$ in 0.1 M KCl solution. After the mixing of these solutions at volume ratios of 1:100, 1:10, 1:1, 10:1, and 100:1, each mixture solution was poured into the polycarbonate wall of the Bio-LSI chip with 40-μm-diameter Au electrodes to measure the electrode potential. In order to input the reference potential into the system, at least one of the 400 electrodes should be set to the V1 mode. Figure S2A shows the typical transients of the rest potentials of an electrode after the potential of the electrodes of the V1 mode was set. Constant rest potentials were observed in accordance with the concentration ratio of $[Fe(CN)_6]^{3-}$/ $[Fe(CN)_6]^{4-}$. Drifts of the electrode potential were typically within 1 mV. We selected 100 electrodes that were in the area far from the V1-mode electrodes on the chip and measured the rest potentials. Figure S2B shows plots of the averaged rest potentials of these 100 electrodes 30 s after the measurements versus the concentration ratio of $[Fe(CN)_6]^{3-}$/ $[Fe(CN)_6]^{4-}$, as well as the theoretical line calculated from equation (1). The error bars indicate ±standard deviations of the data taken from the 100 electrodes. To make a theoretical line, we used E_0 = 0.2396 V according to a cyclic voltammogram of the $[Fe(CN)_6]^{3-}$/ $[Fe(CN)_6]^{4-}$ solution. As shown in Figure 6B, we obtained very uniform rest potentials that agreed with the theoretical value. This result indicates that 2G Bio-LSI can be used as a highly reliable arrayed electrometer. Electrometers can be used for measurements to detect changes in the ratio of the redox species, as indicated in equation (S1). Compared to amperometry, measurements using an electrometer have an advantage in that the redox species are not consumed at the electrode. This advantage is effective when we want to detect very small amounts of a

chemical spice that is produced and consumed, such as the oxygen consumption of a single cell.

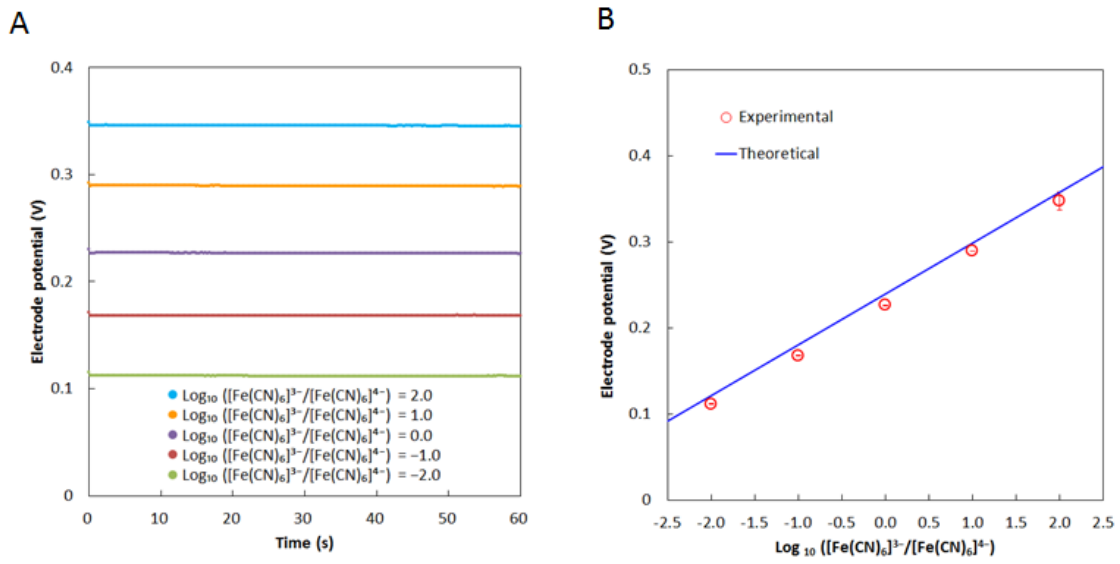

Figure S2. (A) Typical transients of the electrode potential using the electrometer mode of 2G Bio-LSI. (B) Plots of averaged rest potentials of 100 electrodes on a chip versus the concentration ratio of $[Fe(CN)_6]^{3-}$/ $[Fe(CN)_6]^{4-}$ (red circle). We utilized the data obtained after 30 s from the potential step of the V1-mode electrode. The error bars indicate ±standard deviations of the data obtained from the 100 electrodes. The blue line represents a theoretical curve obtained from the Nernst equation.

Electrochemical behavior of H_2O_2 , Na_2SO_3 and dissolved O_2 in PBS solution

We checked the electrochemical behavior of H_2O_2 and Na_2SO_3 and dissolved O_2 in PBS solution using cyclic voltammetry, before we perform the demonstration of the simultaneous detection of O_2 and H_2O_2 shown in Figure 6. A Pt disc electrode (BSA Inc, Japan; diameter=1.0 mm), a Pt plate (3 × 12 mm, thickness = 0.1 mm) and a Ag|AgCl|

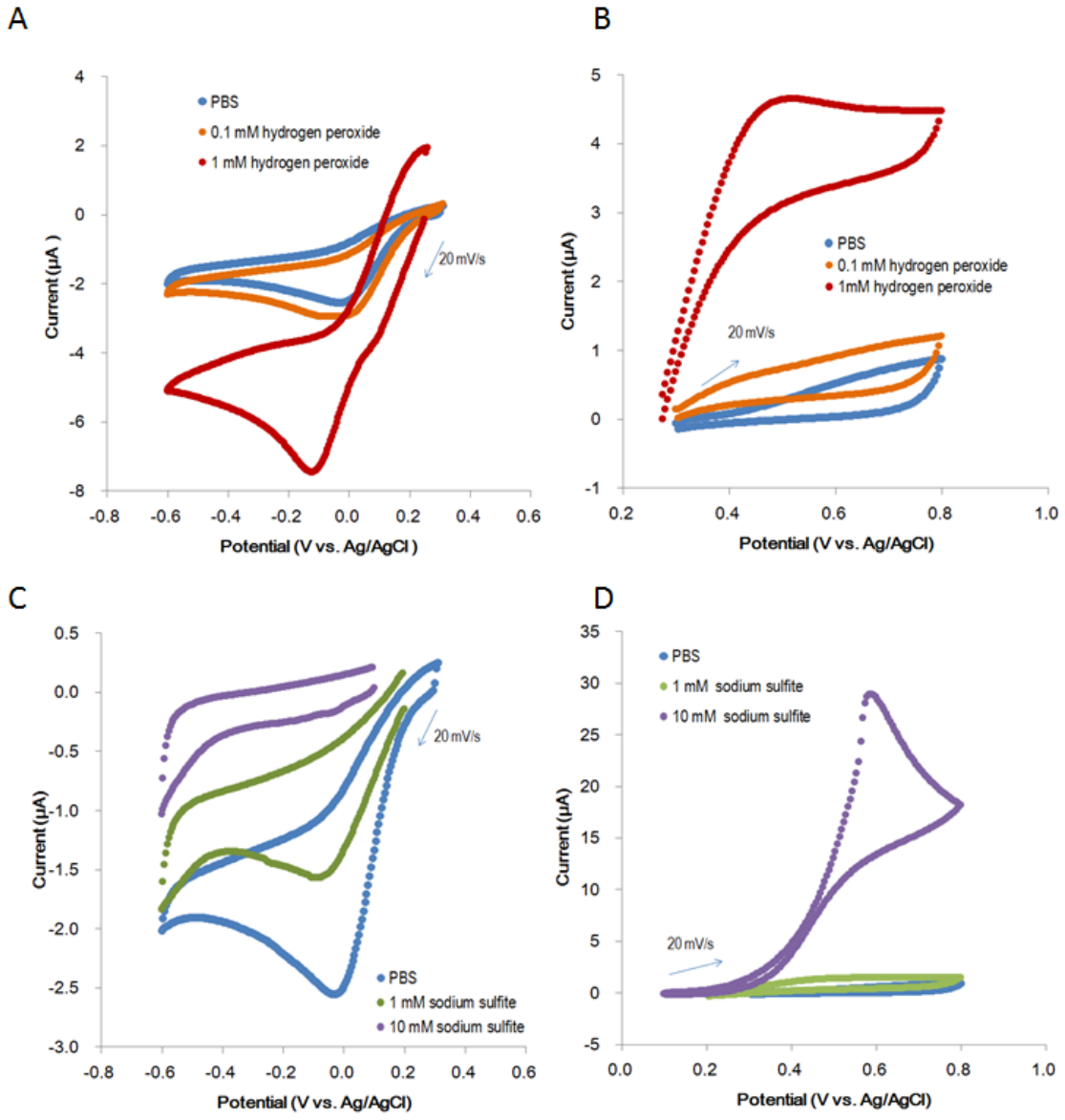

Figure S3. Cyclic voltammograms obtained with Pt disc electrode (1.6 mm in diameter) for the purpose of checking the electrochemical behavior of H_2O_2 and Na_2SO_3 and dissolved O_2 in PBS solution before the demonstration of the simultaneous detection of O_2 and H_2O_2 shown in Figure 6.

sat.KCl electrode were used as the working, counter and reference electrodes, respectively. Voltammetric measurements were carried out using a potentiostat (CompactStat, Ivium Technologies, Netherlands). A Dulbecco's phosphate buffer saline not include Ca^{2+} and Mg^{2+} (Wako Pure Chemical Industries, Japan ; PBS) was used as a electrolyte solution. Scan rate was 20 mV/s. Figure S3 shows resulting voltammograms. The reduction current peak of dissolved O_2 and H_2O_2 were observed at 0.0 V and −0.1 V *vs.* Ag/AgCl, respectively (Figure S3A). The oxidation current peak of H_2O_2 was observed around 0.5 V *vs.* Ag/AgCl (Figure 3B). From these results, we decided to use −0.5 V and 0.7 V *vs.* Ag/AgCl as detection potentials of O_2 and H_2O_2, respectively. The reduction current of dissolved O_2 was decreased with the addition of Na_2SO_3 (Figure S3C), because Na_2SO_3 chemically reduces the dissolved O_2. The reduction current of dissolved O_2 was almost disappeared with 10 mM Na_2SO_3.

As the H_2O_2 is reduced at −0.5 V *vs.* Ag/AgCl, the H_2O_2 reached to the left side of the sensor area (shown red in Figure 6A) generates the reduction current. Figure 4S A and B are identical images to the image of 20 s and 25 s of Figure 6C but different in range of the color bar, respectively. These images clearly show the reduction current derived from the reduction of H_2O_2 reached to the left side as a black semicircle.

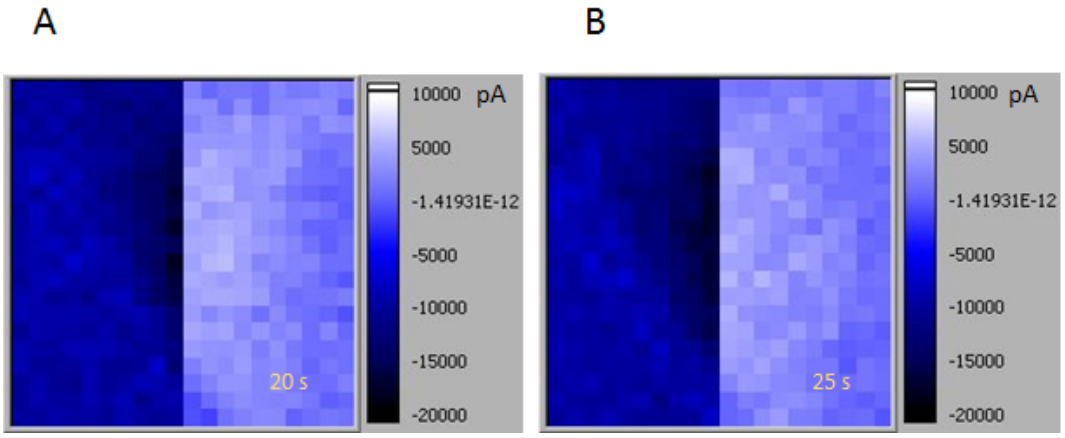

Figure S4. Color maps identical to the images of 20 s (A) and 25 s (B) of Figure 6C in main manuscript but different in range of the color bar.